Radiology: Cardiothoracic Imaging

ORIGINAL RESEARCH

Clinical Validation of the Accuracy of Absolute Myocardial Blood Flow Quantification with Dual-Source CT Using ^{15}O-Water PET

Masafumi Takafuji, MD • Kakuya Kitagawa, MD, PhD • Masaki Ishida, MD, PhD • Yasutaka Ichikawa, MD, PhD • Satoshi Nakamura, MD • Shiro Nakamori, MD, PhD • Tairo Kurita, MD, PhD • Kaoru Dohi, MD, PhD • Hajime Sakuma, MD, PhD

From the Department of Radiology (M.T., K.K., M.I., Y.I., S. Nakamura, H.S.) and Department of Cardiology and Nephrology (S. Nakamori, T.K., K.D.), Mie University Hospital, 2-174 Edobashi, Tsu, Mie 514-8507, Japan. Received March 4, 2021; revision requested April 1; revision received September 11; accepted September 27. **Address correspondence to** M.I. (e-mail: *mishida@clin.medic.mie-u.ac.jp*).

Supported in part by a departmental research grant from Bayer Yakuhin.

Conflicts of interest are listed at the end of this article.

Radiology: Cardiothoracic Imaging 2021; 3(5):e210060 • https://doi.org/10.1148/ryct.2021210060 • Content codes: CT CA

Purpose: To determine the fitting equation that can correct for the underestimation of myocardial blood flow (MBF) measurement by using dynamic CT perfusion (CTP) with dual-source CT (MBF_{CT}), using MBF with oxygen 15–labeled water (^{15}O-water) PET (MBF_{PET}) as a reference, and to determine the accuracy of corrected MBF_{CT} ($MBF_{CT\text{-}corrected}$) compared with MBF_{PET} in a separate set of participants.

Materials and Methods: In this prospective study (reference no. 2466), 34 participants (mean age, 70 years ± 8 [standard deviation]; 27 men) known or suspected to have coronary artery disease underwent dynamic stress CTP and stress ^{15}O-water PET between January 2014 and December 2018. The participants were randomly assigned to either a pilot group (n = 17), to determine the fitting equation on the basis of the generalized Renkin-Crone model that can explain the relation between MBF_{CT} and MBF_{PET}, or to a validation group (n = 17), to validate $MBF_{CT\text{-}corrected}$ compared with MBF_{PET}. The agreement between $MBF_{CT\text{-}corrected}$ and MBF_{PET} was evaluated by intraclass correlation and Bland-Altman analysis.

Results: In the pilot group, MBF_{CT} was lower than MBF_{PET} (1.24 mL/min/g ± 0.28 vs 2.51 mL/min/g ± 0.89 , $P < .001$) at the segment level. The relationship between MBF_{CT} and $MBF_{CT\text{-}corrected}$ was represented as $MBF_{CT} = MBF_{CT\text{-}corrected} \times \{1-\exp[-(0.11 \times MBF_{CT\text{-}corrected} + 1.54)/MBF_{CT\text{-}corrected}]\}$. In the validation group, $MBF_{CT\text{-}corrected}$ was 2.66 mL/min/g ± 1.93, and MBF_{PET} was 2.68 mL/min/g ± 1.87 at the vessel level. $MBF_{CT\text{-}corrected}$ showed an excellent agreement with MBF_{PET} (intraclass correlation coefficient = 0.93 [95% CI: 0.87, 0.96]). The measurement bias of $MBF_{CT\text{-}corrected}$ and MBF_{PET} was –0.02 mL/min/g ± 0.74.

Conclusion: Underestimation of MBF by CT was successfully corrected with a correction method that was based on contrast kinetics in the myocardium.

Supplemental material is available for this article.

Advances in CT systems and postprocessing in the past decade have enabled the use of CT for comprehensive assessment of anatomic stenosis and its hemodynamic significance for myocardial perfusion within a single noninvasive examination (1,2). Dynamic CT perfusion (CTP) with dual-source CT allows quantitative assessment of myocardial perfusion with the maximal upslope method using commercially available software (3). Quantitative estimation of regional stress myocardial blood flow (MBF) obtained with dual-source dynamic CTP using the maximal upslope method (MBF_{CT}) has been shown to be effective for detecting hemodynamically significant coronary artery disease (CAD) (4–6). However, quantification of MBF with dual-source dynamic CTP has not yet been clinically validated.

Absolute MBF can be quantified with PET in milliliters per minute per gram. In particular, oxygen 15–labeled water (^{15}O-water) PET is the most accurate method for quantifying absolute MBF because ^{15}O-water is a metabolically inert, freely diffusible tracer with a 100% extraction fraction over a wide range of blood flows (7). Previous ^{15}O-water PET studies have demonstrated that MBF during vasodilator stress is 3–5 mL/min/g in healthy individuals (8,9). Quantitative ^{15}O-water PET provides high diagnostic performance for predicting CAD. A previous international multicenter study demonstrated that sensitivity, specificity, and accuracy of stress MBF_{PET} for detecting significant CAD were 89%, 84%, and 86%, respectively, at a per-patient level, using optimal cutoff values of 2.3 mL/min/g (10). Recent studies have shown that global stress MBF has important prognostic implications for the risk stratification of patients suspected of having CAD (11,12).

Previous studies of dynamic CTP using the maximal upslope method reported stress MBF of 0.9–1.7 mL/min/g in normal myocardium (4–6,13). The upper limit of this range is substantially lower than that obtained in

Abbreviations

ATP = adenosine triphosphate, CAD = coronary artery disease, CCTA = coronary CT angiography, CTP = CT perfusion, E = extraction fraction, ICC = intraclass correlation coefficient, LoA = limits of agreement, MBF = myocardial blood flow, MBF_{CT} = CT-derived MBF, $MBF_{CT\text{-}corrected}$ = MBF_{CT} after correction with the fitting curve, MBF_{PET} = PET-derived MBF

Summary

True myocardial blood flow can be accurately estimated from dynamic dual-source CT perfusion data using a correction method that is based on contrast kinetics in the myocardium.

Key Points

- Maximal upslope analysis of CT perfusion (CTP) underestimated myocardial blood flow (MBF) compared with oxygen 15–labeled water (^{15}O-water) PET (1.24 mL/min/g ± 0.28 vs 2.51 mL/min/g ± 0.89, $P < .001$).
- In a validation group, use of the correction method more accurately estimated MBF with CTP (2.64 mL/min/g ± 1.94 [corrected] vs 2.67 mL/min/g ± 1.87 [^{15}O-water PET], $P = .88$).
- MBF with CTP corrected with the relationship equation showed excellent agreement with true MBF with ^{15}O-water PET in a separate group (intraclass correlation coefficient = 0.93).

Keywords

CT, CT-Perfusion, PET, Cardiac, Heart

previous ^{15}O-water PET studies, and therefore CT may have underestimated stress MBF. According to the results of a previous study, the underestimation is because MBF_{CT} is not a true MBF, but rather a blood-to-myocardium transfer constant (ie, K1) (14). If true MBF could be obtained with MBF_{CT}, CTP using the maximal upslope method and commercially available software might allow comparison of the MBF values determined with different modalities such as CT and PET and might provide prognostic information. In the single-tissue compartment model, K1 is related to extraction fraction (E) and MBF, and E is dependent on MBF (generalized Renkin-Crone equation) (15–17). Therefore, after the relationship between ^{15}O-water PET–derived true MBF (MBF_{PET}) and MBF_{CT} (ie, K1) has been determined, MBF_{CT} can be converted to true MBF.

The objectives of this study were to determine the fitting curve based on a generalized Renkin-Crone model that can convert MBF_{CT} to true MBF ($MBF_{CT\text{-}corrected}$), using MBF_{PET} as a reference, and to validate the accuracy of $MBF_{CT\text{-}corrected}$ compared with MBF_{PET} in a separate set of participants.

Materials and Methods

Participants

This prospective, single-center study was approved by the institutional review board in our institution (reference no. 2466), and written informed consent for participation in the study was given by all participants. The inclusion criteria were *(a)* participants suspected or known to have CAD and *(b)* age of 45–85 years. The exclusion criteria were *(a)* participants with contraindication to iodinated contrast agents or adenosine triphosphate (ATP), *(b)* participants with persistent atrial fibrillation, and *(c)* participants with acute chest pain or unstable general condition. Stress CTP and ^{15}O-water PET were performed in 36 participants at a median interval of 51 days (interquartile range, 30–73 days) between January 2014 and December 2018. Stress CTP was performed before ^{15}O-water PET in all participants. After excluding one participant who underwent a revascularization procedure and one who changed medication between the two scans, 34 participants (27 men and seven women; mean age, 70 years ± 8) were randomly assigned to either a pilot group ($n = 17$), to determine the fitting curve that can convert MBF_{CT} to $MBF_{CT\text{-}corrected}$ using MBF_{PET} as a reference, or a validation group ($n = 17$), to validate $MBF_{CT\text{-}corrected}$ against MBF_{PET} (Fig 1). All participants refrained from caffeine intake 24 hours before stress CTP and ^{15}O-water PET (18). No participants received medication suppressing maximal responses to ATP-mediated vasodilator stress, such as theophylline (19). Heart rate, electrocardiogram, and blood pressure were monitored during the examinations.

CT Protocol and Quantification of MBF_{CT}

CT examinations were performed using dual-source CT scanners (SOMATOM Definition Flash or SOMATOM Force; Siemens Healthineers). The CT protocol comprised stress dynamic CTP, followed by coronary CT angiography (CCTA) and CT delayed enhancement (2,4,20,21) (Fig 2). Contrast agent and ATP administration, image acquisition methods, and image analysis for CT examinations are explained in Appendix E2 (supplement). For stress dynamic CTP, briefly, MBF_{CT} was calculated from the maximum upslope of the time-attenuation curves for every voxel using commercially available software (*syngo*.via; Siemens Healthineers). The MBF_{CT} values in 16 segments (ie, the American Heart Association model's 17 segments except for the apex) were obtained from the MBF_{CT} map.

^{15}O-Water PET Protocol and Quantification of MBF_{PET}

^{15}O-water PET was performed at rest and during vasodilator stress using a PET/CT scanner (Discovery PET/CT 690 VCT; GE Medical Systems). Acquisition methods and image analysis are explained in Appendix E3 (supplement). Stress MBF was measured by a standard single-tissue compartment model with correction for perfusable tissue fraction on the American Heart Association 17-segment model.

Formula for Calculation of $MBF_{CT\text{-}Corrected}$ and Validation of $MBF_{CT\text{-}Corrected}$ against MBF_{PET}

Segments out of the scan range on the dynamic CTP images (20) and segments with a thickness of less than 5 mm (22,23) were excluded from the analysis.

In the pilot group, the correlations between the permeability–surface-area product values of iodinated contrast medium and MBF_{PET} were determined from MBF_{CT} and MBF_{PET} using linear analysis, and parameters α and β were estimated using Equations (E8)–(E10) in Appendix E1 (supplement) (15–17). In the pilot group, segments in which MBF_{PET} was less than MBF_{CT} were excluded from analysis because the Renkin-Crone equation (Eq [E9]

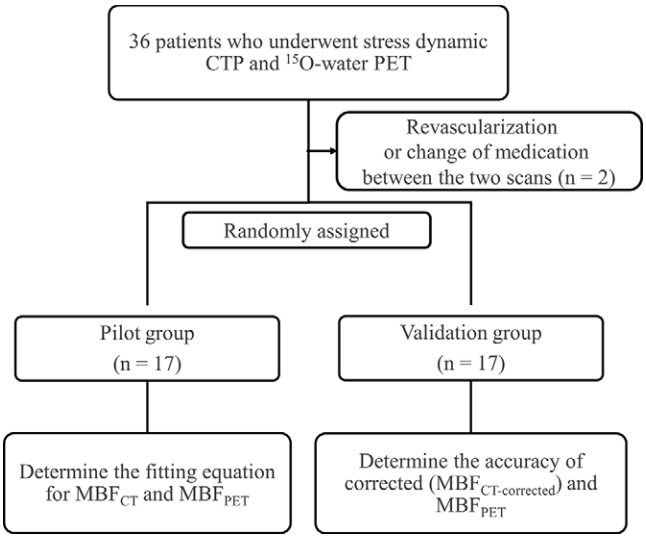

Figure 1: Overview of the study design including participant selection protocol. CTP = CT perfusion, MBF = myocardial blood flow, MBF_{CT} = CT-derived MBF, $MBF_{CT\text{-}corrected}$ = corrected MBF_{CT}, MBF_{PET} = PET-derived MBF, ^{15}O-water = oxygen 15–labeled water.

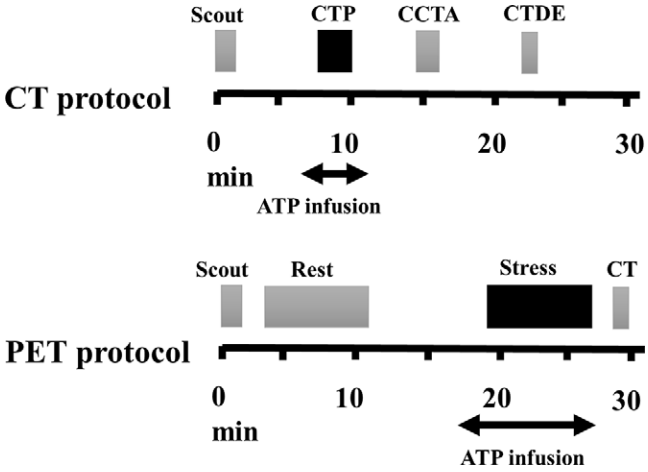

Figure 2: Flowchart of image acquisition protocols. The CT protocol consisted of stress dynamic CT perfusion (CTP), followed by coronary CT angiography (CCTA) and CT delayed enhancement (CTDE). The PET protocol consisted of rest and stress examinations and helical CT for attenuation correction. In both protocols, pharmacologic vasodilator stress was performed with intravenous infusion of adenosine triphosphate (ATP; 0.16 mg/kg/min).

in Appendix E1 [supplement]) does not allow that MBF_{PET} can be less than MBF_{CT}. The relationship between E and MBF_{PET} was determined by substituting the simple linear correlation between permeability–surface-area product and MBF obtained by the linear regression analysis into the generalized Renkin-Crone equation (Eq [E11] in Appendix E1 [supplement]).

Statistical Analysis

The sample size (segments) was calculated using a Pearson correlation coefficient with an α probability of .05 and power of 0.80. We defined a null hypothesis as ρ = 0.55 as a criterion for moderate correlation and an alternative hypothesis as ρ = 0.67 (24). Target sample size was 215 segments. Expecting an exclusion rate of 20% at segmental level, 272 segments (17 participants) were required for each group. Continuous variables are expressed as the mean ± standard deviation, and categorical variables are expressed as proportions. Student *t* test was used to assess differences in continuous variables after examining the normality of the data. The χ^2 test was used to assess the differences in proportion between categorical variables. In the validation group, the relationship between MBF_{CT} and MBF_{PET} and between $MBF_{CT\text{-}corrected}$ and MBF_{PET} were assessed using Pearson correlation coefficient and linear regression analysis. The degree of agreement between $MBF_{CT\text{-}corrected}$ and MBF_{PET} was evaluated according to the Bland-Altman method, percent difference, intraclass correlation coefficient (ICC), and equivalence test. The percent difference was defined as 100 × (difference of the tests)/(mean of the tests). The equivalence test was performed using two one-sided *t* tests (25). The two one-sided *t* tests are constructed for the null hypotheses that the true difference exceeds the equivalent criteria. If both tests reject (ie, $P < .05$), the groups are considered practically equivalent. The greatest of these *P* values was taken to evaluate the equivalence. The equivalence criteria were *(a)* within 15% at the participant level and *(b)* 30% at the vessel and segment levels according to the range of variability of the MBF_{PET} measurements in previous studies (26,27). All statistical analyses were performed using JMP version 10 software (SAS Institute). Values of *P* less than .05 were considered to indicate statistical significance.

Results

Participant Characteristics

There were no significant differences in sex, age, body mass index, risk factors for CAD, smoking, medication, history of CAD, coronary calcium score, number of diseased vessels at CCTA, or Coronary Artery Disease Reporting and Data System score between the pilot and validation groups (Table). No serious adverse reaction was recorded in any examination. Heart rate increased with ATP administration from 66 beats per minute ± 10 (range, 50–90 beats per minute) to 79 beats per minute ± 12 (range, 59–100 beats per minute) at dynamic CTP ($P < .001$) and from 69 beats per minute ± 11 (range, 52–95 beats per minute) to 77 beats per minute ± 12 (range, 55–100 beats per minute) at ^{15}O-water PET ($P < .001$).

The dose-length product of dynamic CTP, CCTA, and CT delayed enhancement was 270 mGy·cm ± 78, 202 mGy·cm ± 117, and 116 mGy·cm ± 43, respectively; the effective dose for the three techniques was 3.77 mSv ± 1.10, 2.83 mSv ± 1.64, and 1.62 mSv ± 0.60, respectively.

Segments Excluded from MBF Analysis in the Pilot and Validation Groups

In the pilot group, 26 of the 272 segments (9.6%) were excluded: 13 segments with a thickness of less than 5 mm (4.8%) and 13 segments with an MBF_{PET} less than MBF_{CT} (4.8%). No segment was out of the scan range.

In the validation group, 18 of the 272 segments (6.6%) were excluded: 12 segments with a thickness of less than 5 mm (4.4%) and six segments out of the scan range (2.2%).

Participant Characteristics

Characteristic	Pilot Group (n = 17)	Validation Group (n = 17)	P Value
No. of men	14 (82%)	13 (76%)	.67
Age (y)			
Mean ± SD	68.6 ± 6.8	71.1 ± 9.0	.36
Median	70	72	
Interquartile range	62–74	70–76	
Range	56–78	48–81	
Body mass index (kg/m^2)			
Mean ± SD	23.8 ± 5.1	24.8 ± 4.6	.55
Median	22	25	
Interquartile range	21–26	21–27	
Range	16.8–38.0	18.4–34.9	
Risk factors for CAD			
Hypertension	10 (59%)	13 (76%)	.27
Hyperlipidemia	11 (65%)	11 (65%)	>.99
Diabetes	7 (41%)	11 (65%)	.17
Family history of CAD	5 (29%)	4 (24%)	.70
Smoking			.15
Those who have never smoked	9 (53%)	4 (24%)	
Those with smoking history	4 (24%)	9 (53%)	
Those who currently smoke	4 (24%)	4 (24%)	
Medication			
ACE-I or ARB	7 (41%)	11 (65%)	.17
β-blockers	5 (29%)	2 (12%)	.20
Calcium channel blockers	5 (29%)	7 (41%)	.47
Aspirin	9 (53%)	10 (59%)	.73
Nitrate	4 (24%)	1 (6%)	.17
Statin	8 (47%)	8 (47%)	>.99
Theophylline	0 (0%)	0 (0%)	>.99
History of CAD			
History of myocardial infarction	4 (24%)	3 (18%)	.67
Prior PCI	5 (29%)	5 (29%)	>.99
Prior CABG	1 (6%)	2 (12%)	.55
Coronary calcium score			
Mean ± SD	1280 ± 2086	1091 ± 1296	.81
Median	156	581	
Interquartile range	19–2209	2–1977	
Range	10–6879	0–3357	
Vessel disease at CTA			.94
No vessel disease	3 (18%)	2 (12%)	
One-vessel disease	4 (24%)	4 (24%)	
Two-vessel disease	2 (12%)	3 (18%)	
Three-vessel disease	8 (47%)	8 (47%)	
CAD-RADS score			.50
0	0 (0%)	1 (6%)	
1	2 (12%)	1 (6%)	

Table (*continues*)

Table (*continued*): Participant Characteristics

Characteristic	Pilot Group (n = 17)	Validation Group (n = 17)	P Value
2	2 (12%)	0 (0%)	
3	3 (18%)	1 (6%)	
4A	3 (18%)	5 (29%)	
4B	3 (18%)	5 (29%)	
5	4 (24%)	4 (24%)	

Note.—Except where otherwise noted, data are presented as the numbers of participants, with percentages in parentheses. Student t test was used to assess differences in continuous variables. The χ^2 test was used to assess the differences in proportion between categorical variables. ACE-I or ARB = angiotensin-converting enzyme inhibitor or angiotensin II receptor blocker, CABD = coronary artery bypass graft, CAD = coronary artery disease, CAD-RADS = Coronary Artery Disease Reporting and Data System, CTA = CT angiography, PCI = percutaneous coronary intervention, SD = standard deviation.

Formula for Calculation of $MBF_{CT\text{-}Corrected}$ in the Pilot Group

The mean MBF_{CT} was 1.24 mL/min/g ± 0.28, and mean MBF_{PET} was 2.51 mL/min/g ± 0.89 in the pilot group at the segment level. The relationship between MBF_{CT} and MBF_{PET} is shown in Figure 3. The parameters α (.11) and β (1.54) were estimated from these data using Equations (E8)–(E10) (Appendix E1 [supplement]). The relationships between E, MBF_{CT}, and $MBF_{CT\text{-}corrected}$ were expressed as

$$E = 1 - e^{-\frac{(0{,}11 \times MBF + 1.54)}{MBF}} \quad (1),$$

$$MBF_{CT} = (1 - 0.90e^{-\frac{1.54}{MBF}}) \times MBF \quad (2),$$

and

$$MBF_{CT\text{-}corrected} = \frac{1.54MBF^{CT}}{MBF^{CT} \times W^{0}\left(\frac{1.39e^{-\frac{1.54}{MBF^{CT}}}}{MBF^{CT}}\right)} \quad (3).$$

Accuracy of $MBF_{CT\text{-}Corrected}$ in the Validation Group

Before correction in the validation group, MBF_{CT} was underestimated compared with MBF_{PET}: Mean MBF_{CT} and MBF_{PET} were 1.24 mL/min/g ± 0.33 and 2.67 mL/min/g ± 1.87 at the participant level (P = .002), 1.24 mL/min/g ± 0.33 and 2.68 mL/min/g ± 1.87 at the vessel level (P < .001), and 1.25 mL/min/g ± 0.36 and 2.70 mL/min/g ± 1.93 at the segment level (P < .001), respectively. After the correction using the relationship obtained in the pilot group, no significant difference was observed between $MBF_{CT\text{-}corrected}$ and MBF_{PET}. Mean $MBF_{CT\text{-}corrected}$ was 2.64 mL/min/g ± 1.94 at the participant level (P = .88), 2.66 mL/min/g ± 1.93 at the vessel level (P = .85), and 2.70 mL/min/g ± 2.02 at the segment level (P = .99) (Fig 4).

There was excellent linear correlation between $MBF_{CT\text{-}corrected}$ and MBF_{PET} at the participant level (y = 0.97x + 0.06, r = 0.93 [95% CI: 0.81, 0.97]; P < .001), vessel level (y = 0.96x + 0.09, r = 0.92 [95% CI: 0.87, 0.96]; P < .001), and segment level (y = 0.94x + 0.16, r = 0.90 [95% CI: 0.87, 0.92]; P < .001). ICC between $MBF_{CT\text{-}corrected}$ and MBF_{PET} was 0.93 (95% CI: 0.82, 0.98), 0.93 (95% CI: 0.87, 0.96), and 0.90 (95% CI: 0.87, 0.92) at the participant, vessel, and segment levels, respectively (Fig 5A).

Bland-Altman plots showed a mean difference between $MBF_{CT\text{-}corrected}$ and MBF_{PET} of –0.03 mL/min/g ± 0.72 (95% limits of agreement [LoA], –1.44 to 1.38 mL/min/g) at the participant level, –0.02 mL/min/g ± 0.74 (95% LoA, –1.48 to 1.44 mL/min/g) at the vessel level, and 0.001 mL/min/g ± 0.90 (95% LoA, –1.77 to 1.77) at the segment level (Fig 5B). The percent difference between $MBF_{CT\text{-}corrected}$ and MBF_{PET} was –4% ± 23, –4% ± 24, and –4% ± 30, at the participant, vessel, and segment levels, respectively. Using the criteria based on ^{15}O-water PET interstudy variability, $MBF_{CT\text{-}corrected}$ demonstrated an equivalence to MBF_{PET} at the vessel (P = .02) and segment levels (P < .001), but not at the participant level (P = .29). A representative participant is presented in Figure 6.

Discussion

In this study, we determined an equation representing the relationship between MBF_{CT} and MBF_{PET} that was based on the generalized Renkin-Crone model in the pilot group. When the correction equation was applied in the validation group, $MBF_{CT\text{-}corrected}$ showed excellent agreement with MBF_{PET}.

Quantitative assessment of dual-source dynamic CTP enables quantification of MBF. However, the MBF value determined by CTP is influenced by the characteristics of the contrast medium (14). Most importantly, MBF quantified with dual-source CTP and commercially available software (MBF_{CT}) is based on the rate of contrast enhancement in myocardial tissue compared with that in the blood pool at the peak of blood contrast enhancement and equals K1, not true MBF (14). Because E of contrast medium from capillary blood to the extracellular space is less than 1.0, underestimation of MBF is inevitable. The noncorrected CT perfusion measure (MBF_{CT}; ie, K1) was markedly attenuated in higher MBF relative to ^{15}O-water PET in our study. The underestimation of MBF_{CT} in higher MBF depends on characteristics of iodinated contrast medium as the perfusion tracer. The underestimation of MBF_{CT} in higher MBF may

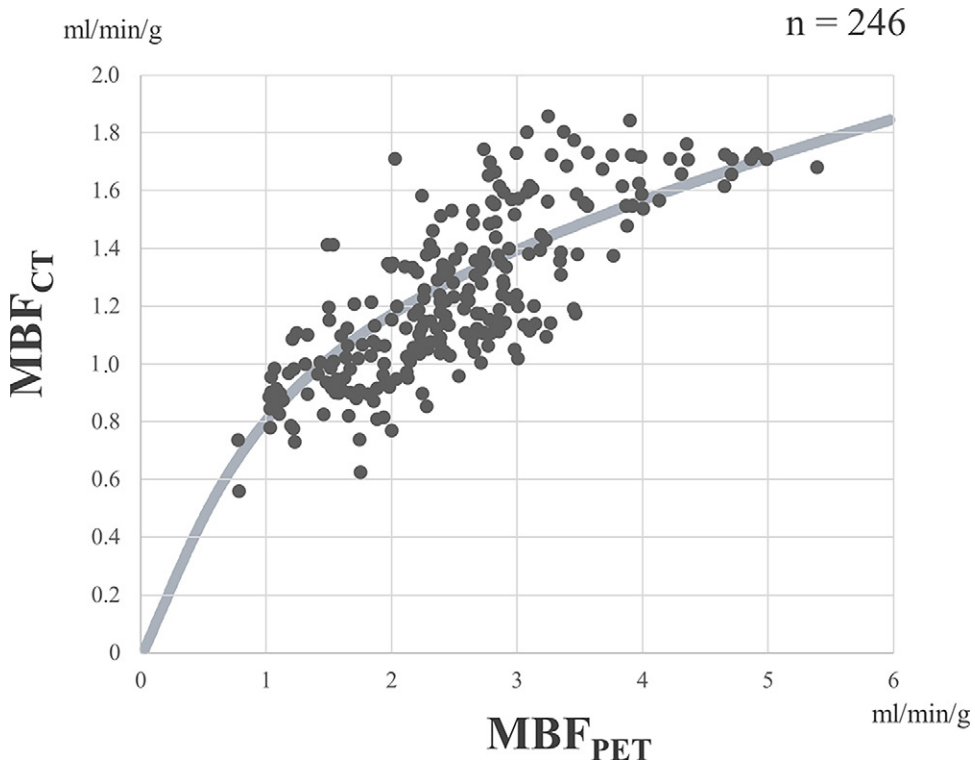

Figure 3: Relationship between MBF_{CT} and MBF_{PET} in the pilot group. MBF = myocardial blood flow, MBF_{CT} = CT-derived MBF, MBF_{PET} = PET-derived MBF.

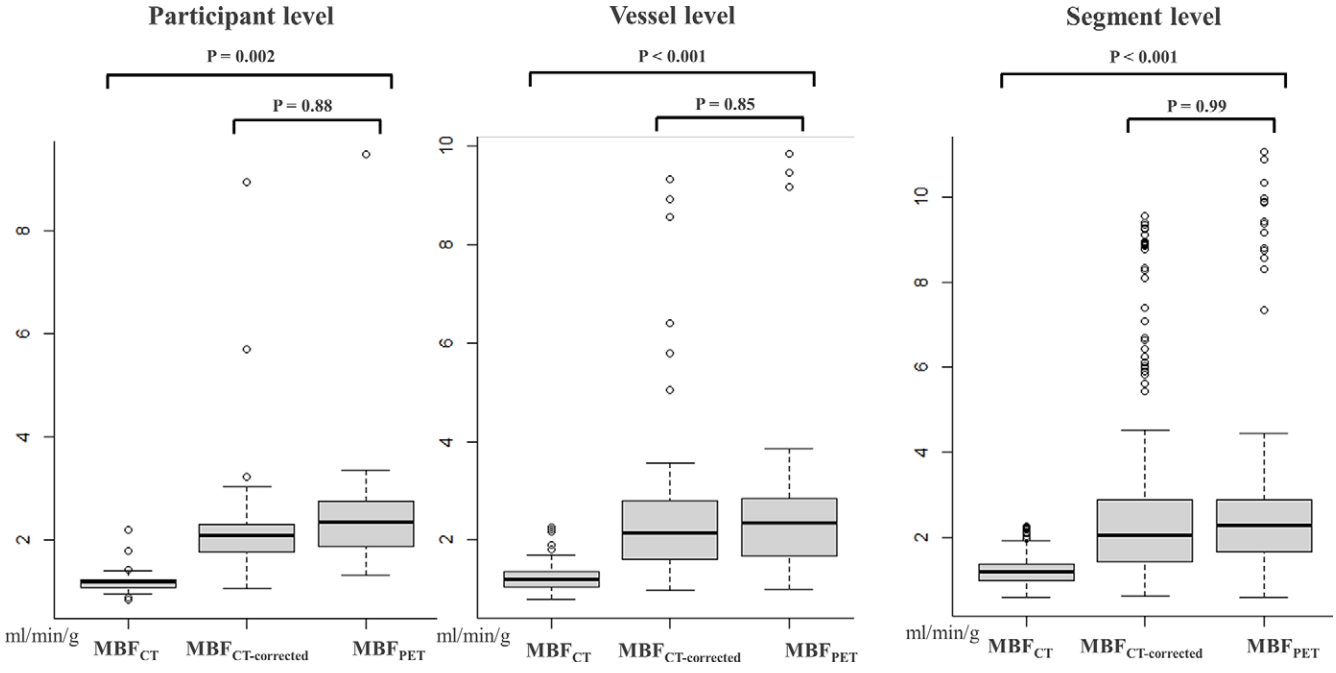

Figure 4: MBF_{CT} was significantly underestimated compared with MBF_{PET} at the participant, vessel, and segment levels, whereas with correction using the relationship obtained in the pilot group, no significant difference was observed between $MBF_{CT-corrected}$ and MBF_{PET} at the participant, vessel, or segment levels. MBF = myocardial blood flow, $MBF_{CT-corrected}$ = CT-derived MBF after correction with the fitting curve, MBF_{CT} = CT-derived MBF, MBF_{PET} = PET-derived MBF.

lead to discordance of the value of stress MBF value. However, our correction method enables appropriate interpretation of the absolute stress MBF derived from CTP, allowing for the understanding of the implication of stress MBF between multiple modalities, including ^{15}O-water PET.

In the current study, we first determined the fitting equation that describes the relation between MBF_{CT} and MBF_{PET} by using the generalized Renkin-Crone model, employing ^{15}O-water PET as the reference standard for MBF. The E of iodinated contrast medium was described as E = 1 – 0.90 exp (–1.54/MBF) in

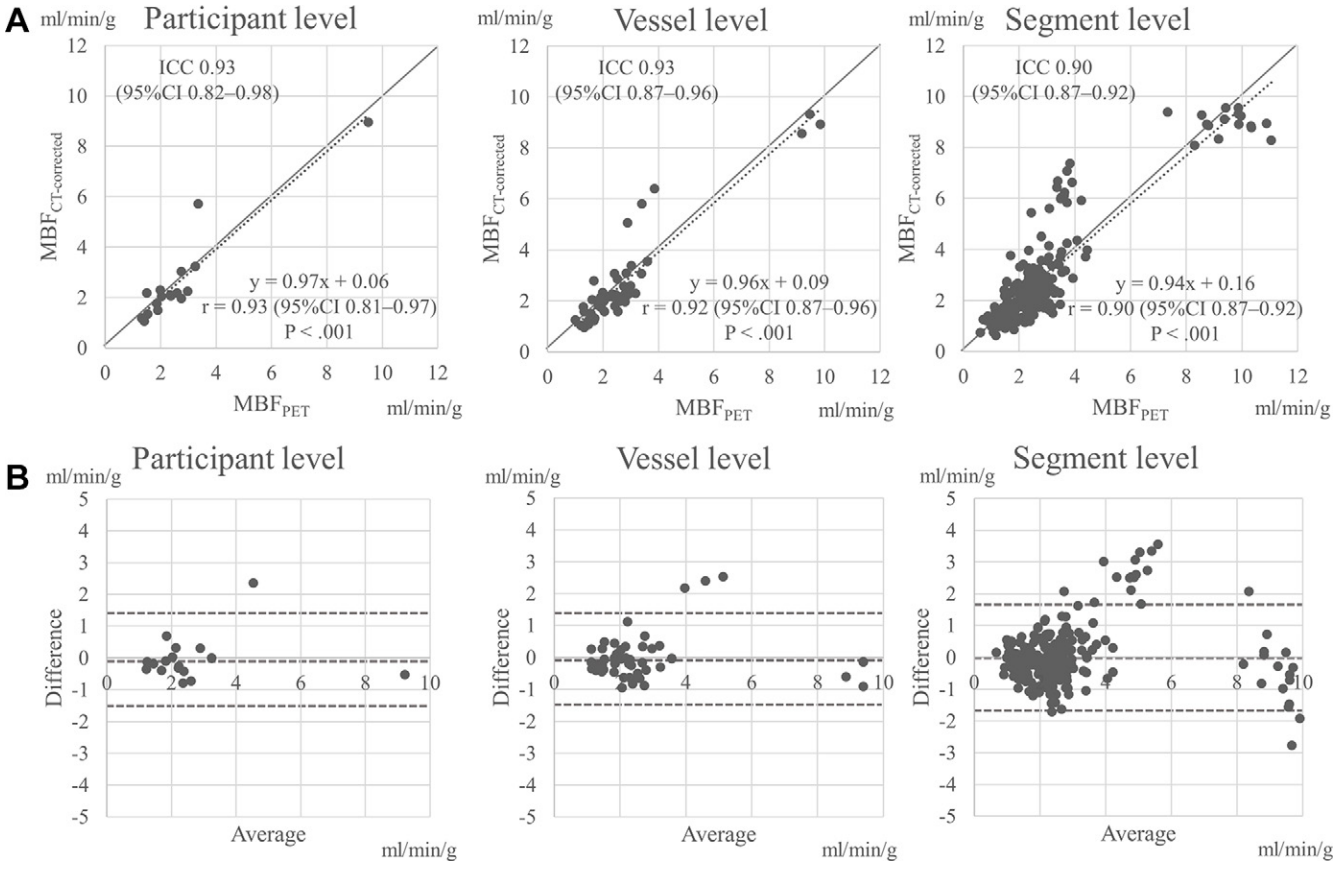

Figure 5: **(A)** Intraclass correlation coefficients (ICCs) and correlations between $MBF_{CT\text{-}corrected}$ and MBF_{PET} at the patient, vessel, and segment levels were excellent. Dashed line indicates line of best fit for linear regression. Solid line indicates line of identity. **(B)** Bland-Altman plots with 95% limits of agreement demonstrate agreement between $MBF_{CT\text{-}corrected}$ and MBF_{PET}. MBF = myocardial blood flow, $MBF_{CT\text{-}corrected}$ = CT-derived MBF after correction with the fitting curve, MBF_{PET} = PET-derived MBF.

the present study and E = 1 – 0.904 exp (–1.203/MBF) (28) in the previous study that employed ^{15}O-water PET as the reference standard for MBF, whereas in previous MRI studies, the E of gadolinium-diethylenetriamine pentaacetic acid was described as E = 1 – 0.87 exp (–0.56/MBF) (17) and E = 1 – 0.892 exp (–0.964/MBF) (29). Thus, the extraction efficiency of iodinated contrast medium is up to 1.1 to approximately 1.6 times higher than gadolinium contrast medium for MBF from 0.5 to 3.0 mL/min/g, which suggests that the property of iodinated contrast medium as a perfusion tracer might provide a more accurate MBF measurement than that of gadolinium contrast medium. Considering that the molecular weight of CT and MRI contrast media are similar, both are inert substances, and passive diffusion is the dominant mechanism for influx from blood to tissue for both, other factors, including the differences in the mechanism of contrast effect and the nonlinearity between signal intensity and contrast concentration in MRI, might affect the difference of apparent extraction efficiency between iodinated and gadolinium contrast medium.

After determining the correction equation in the pilot group, the accuracy of $MBF_{CT\text{-}corrected}$ was compared with MBF_{PET} in a separate validation group. At the vessel level, there was a high linear correlation and low bias, and some variance was noted. The variance might be attributable to potential misregistration of the segments between CTP and ^{15}O-water PET or to the relatively long interval between CTP and ^{15}O-water PET. Nevertheless, the percent difference between $MBF_{CT\text{-}corrected}$ and MBF_{PET} in this study was within the range of the variability of ^{15}O-water MBF measurement (26,27). In addition, the ICC between $MBF_{CT\text{-}corrected}$ and MBF_{PET} was close to that of intraobserver reproducibility of ^{15}O-water PET (0.92 vs 0.90–0.96 at the vessel level) (27). Global stress $MBF_{CT\text{-}corrected}$ also showed excellent agreement with global stress MBF_{PET} and had higher linear correlation and smaller variance compared with vessel-based analysis. These results show an excellent agreement between $MBF_{CT\text{-}corrected}$ and MBF_{PET} both at the vessel and global levels. However, Bland-Altman plots show the substantial variance between CT and PET estimates of MBF at the segment levels. Therefore, the reliability of segmental assessment of MBF with the quantitative perfusion CT approach is to be improved and validated in further studies.

Most clinical evidence on dynamic CTP has been obtained using dual-source CT and the dedicated perfusion quantification software using maximal upslope model (4–6). However, quantitative perfusion measure determined with dual-source CTP has not been validated clinically yet. In the current study, we validated the accuracy of MBF determined with dual-source CTP using ^{15}O-water PET as the reference standard and developed a mathematical correction method to obtain true MBF. This point is the most important clinical relevance in our study. Thus far, there are two studies that have clinically validated MBF with dynamic CTP against myocardial perfusion PET (28,30). However, in contrast to our study, both studies

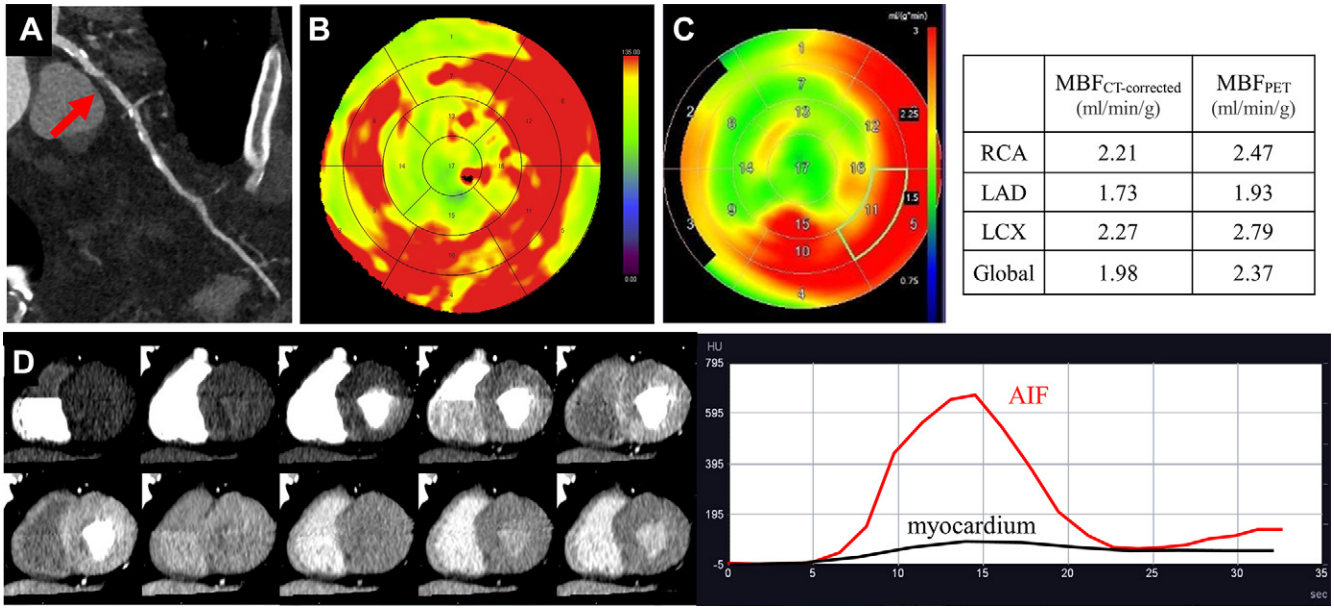

	$MBF_{CT\text{-}corrected}$ (ml/min/g)	MBF_{PET} (ml/min/g)
RCA	2.21	2.47
LAD	1.73	1.93
LCX	2.27	2.79
Global	1.98	2.37

Figure 6: Images in a 72-year-old man with diabetes and hyperlipidemia. **(A)** Coronary CT angiographic image shows severe stenosis (red arrow) in the proximal portion of the left anterior descending artery (LAD). Both the **(B)** MBF_{CT} map and **(C)** MBF_{PET} map demonstrate similar distribution of abnormal perfusion in the anteroseptal wall and apex corresponding to the LAD stenosis. **(D)** The dynamic CT perfusion (CTP) images and time-attenuation curve obtained with dynamic CTP are demonstrated. AIF = arterial input function, LCX = left circumflex artery, MBF = myocardial blood flow, MBF_{CT} = CT-derived MBF, $MBF_{CT\text{-}corrected}$ = CT-derived MBF after correction with the fitting curve, MBF_{PET} = PET-derived MBF, RCA = right coronary artery.

employed the single-source large-coverage scanner. Moreover, the blood flow models used in those studies were different from the one used in our study. Kikuchi et al used curve fitting using the nonlinear least squares with the generalized Renkin-Crone equation (28). Alessio et al used the two-compartment exchange model (30). In contrast, maximal upslope model with correction using the generalized Renkin-Crone equation was used in our study. These technical differences in the type of scanner and mathematical modeling may explain the differences between our study and others.

Recent PET studies have emphasized the value of global stress MBF for the evaluation of prognosis in patients with CAD (11,12). Bom et al (11) demonstrated that global stress MBF with ^{15}O-water PET has prognostic value for predicting cardiovascular events independent of clinical characteristics in patients with CAD. Farhad et al (12) revealed that global stress MBF with rubidium 82 PET was an independent predictor of major adverse cardiac events in patients with CAD, which provided added value to the evaluation of regional ischemia using summed difference score. In this regard, $MBF_{CT\text{-}corrected}$ could serve as an alternative to cardiac PET for the risk stratification of patients with suspected CAD. This is of potential clinical relevance because CT has wider availability and lower cost compared with ^{15}O-water PET, which requires an on-site cyclotron. However, it is still lacking the evidence for the clinical value of global MBF with CTP for the risk stratification of patients with CAD. The value of $MBF_{CT\text{-}corrected}$ for the risk stratification of patients with CAD requires further investigation.

In 2017, Michallek and Dewey demonstrated the importance of perfusion pattern of stress perfusion MR images in patients with chronic ischemic heart disease (31). Compared with MBF quantification, perfusion pattern analysis is another approach to explore the usefulness of stress CTP. Pathophysiologic analysis including quantification of perfusion patterns might have added clinical values even in stress CTP. Further investigation is desirable to address this point.

There were some limitations in the present study. First, there was a relatively long interval between the dynamic CTP and ^{15}O-water PET studies due to scheduling problems concerning scanner availability. However, none of the 34 participants analyzed in this study experienced a cardiac event or underwent a therapeutic intervention in the time between the two studies. Second, we did not evaluate the diagnostic value of our correction method in managing participants with CAD. Further investigation is needed to assess the impact of stress $MBF_{CT\text{-}corrected}$ on diagnosis and value at different institutions with larger populations. Third, in the pilot group, the segments with MBF_{PET} lower than MBF_{CT} were excluded from analysis due to the restriction of the Renkin-Crone equation. This nonphysiologic phenomenon might be related to reproducibility for measuring MBF_{CT}. So far, the test-retest reproducibility for measuring MBF_{CT} remains unknown. Further study is warranted. However, a previous study (4) demonstrated the good intra- and interobserver reproducibility for measuring MBF_{CT} (ICC of 0.934 and 0.913, respectively, at the vessel level) using the same approach employed in our study. This may have an influence in obtaining the equation that converts MBF_{CT} to true MBF. However, the excellent agreement between $MBF_{CT\text{-}corrected}$ and MBF_{PET} in the validation group suggests that the influence will be negligibly small. Fourth, reproducibility was not evaluated in this study. Further investigation will be required regarding the reproducibility of our correction method. Fifth, there is a paucity of data at the lower range of MBF, particularly less than 0.8 mL/min/g, limiting the ability to prove

the validity of the Renkin-Crone formula at the lower range of MBF in our study. However, stress MBF in the segments with transmural infarct were all above 0.8 mL/min/g with ^{15}O-water PET in this study. This is consistent with the result of a previous study using ^{15}O-water PET, where the MBF of infarcted myocardium was 0.82 mL/min/g ± 0.21 at rest and 1.20 mL/min/g ± 0.45 at vasodilator stress (32), indicating that our approach has validity in a reasonable range of stress MBF even in the segment with transmural infarct. Finally, the quantification techniques and fitting curves may vary from system to system. However, when a similar type of CT scanner and injection protocol are employed, fitting curves are generally consistent. Therefore, as long as the dual-source CT scanner, imaging protocol, and injection protocol of contrast medium employed in this study are used, our quantification technique is applicable. So far, to our knowledge, most of the previous dynamic CTP studies employed the dual-source CT scanner, similar imaging protocol, and contrast medium injection protocol as used in our study. In this respect, our quantification method is readily applicable to those widely used dual-source CT protocols.

The relationship between MBF_{CT} and true MBF was determined using ^{15}O-water PET as the reference standard. The new correction method, which was based on contrast kinetics in the myocardium, enabled true MBF to be adequately estimated from dynamic CTP data obtained with dual-source CT, using commercially available software. Underestimation of MBF has long been considered as an important limitation of dynamic CTP with dual-source CT; however, our correction equation may solve this problem and extend the clinical use of quantitative perfusion CT.

Author contributions: Guarantor of integrity of entire study, H.S.; study concepts/study design or data acquisition or data analysis/interpretation, all authors; manuscript drafting or manuscript revision for important intellectual content, all authors; approval of final version of submitted manuscript, all authors; agrees to ensure any questions related to the work are appropriately resolved, all authors; literature research, M.T., M.I., H.S.; clinical studies, M.T., K.K., M.I., Y.I., S. Nakamori, T.K., K.D.; statistical analysis, M.T., S. Nakamura; and manuscript editing, M.T., K.K., M.I., S. Nakamura, H.S.

Disclosures of Conflicts of Interest: **M.T.** No relevant relationships. **K.K.** Endowed chair of Siemens Healthcare KK and Fujifilm Medical; joint research agreement with Elucid Bioimaging; honoraria for lectures from Siemens Healthcare KK. **M.I.** No relevant relationships. **Y.I.** No relevant relationships. **S. Nakamura** No relevant relationships. **S. Nakamori** No relevant relationships. **T.K.** No relevant relationships. **K.D.** No relevant relationships. **H.S.** Departmental research grants with Eisai, Fujifilm Holdings, Guerbet.

References

1. Schuijf JD, Ko BS, Di Carli MF, et al. Fractional flow reserve and myocardial perfusion by computed tomography: a guide to clinical application. Eur Heart J Cardiovasc Imaging 2018;19(2):127–135.
2. Nakamura S, Kitagawa K, Goto Y, et al. Incremental prognostic value of myocardial blood flow quantified with stress dynamic computed tomography perfusion imaging. JACC Cardiovasc Imaging 2019;12(7 Pt 2):1379–1387.
3. Mahnken AH, Klotz E, Pietsch H, et al. Quantitative whole heart stress perfusion CT imaging as noninvasive assessment of hemodynamics in coronary artery stenosis: preliminary animal experience. Invest Radiol 2010;45(6):298–305.
4. Goto Y, Kitagawa K, Uno M, et al. Diagnostic accuracy of endocardial-to-epicardial myocardial blood flow ratio for the detection of significant coronary artery disease with dynamic myocardial perfusion dual-source computed tomography. Circ J 2017;81(10):1477–1483.
5. Bamberg F, Becker A, Schwarz F, et al. Detection of hemodynamically significant coronary artery stenosis: incremental diagnostic value of dynamic CT-based myocardial perfusion imaging. Radiology 2011;260(3):689–698.
6. Coenen A, Lubbers MM, Kurata A, et al. Diagnostic value of transmural perfusion ratio derived from dynamic CT-based myocardial perfusion imaging for the detection of haemodynamically relevant coronary artery stenosis. Eur Radiol 2017;27(6):2309–2316.
7. Klein R, Beanlands RS, deKemp RA. Quantification of myocardial blood flow and flow reserve: Technical aspects. J Nucl Cardiol 2010;17(4):555–570.
8. Uren NG, Melin JA, De Bruyne B, Wijns W, Baudhuin T, Camici PG. Relation between myocardial blood flow and the severity of coronary-artery stenosis. N Engl J Med 1994;330(25):1782–1788.
9. Uren NG, Camici PG, Melin JA, et al. Effect of aging on myocardial perfusion reserve. J Nucl Med 1995;36(11):2032–2036.
10. Danad I, Uusitalo V, Kero T, et al. Quantitative assessment of myocardial perfusion in the detection of significant coronary artery disease: cutoff values and diagnostic accuracy of quantitative [(15)O]H2O PET imaging. J Am Coll Cardiol 2014;64(14):1464–1475.
11. Bom MJ, van Diemen PA, Driessen RS, et al. Prognostic value of [15O]H2O positron emission tomography-derived global and regional myocardial perfusion. Eur Heart J Cardiovasc Imaging 2020;21(7):777–786.
12. Farhad H, Dunet V, Bachelard K, Allenbach G, Kaufmann PA, Prior JO. Added prognostic value of myocardial blood flow quantitation in rubidium-82 positron emission tomography imaging. Eur Heart J Cardiovasc Imaging 2013;14(12):1203–1210.
13. Kim EY, Chung WJ, Sung YM, et al. Normal range and regional heterogeneity of myocardial perfusion in healthy human myocardium: assessment on dynamic perfusion CT using 128-slice dual-source CT. Int J Cardiovasc Imaging 2014;30(Suppl 1):33–40.
14. Ishida M, Kitagawa K, Ichihara T, et al. Underestimation of myocardial blood flow by dynamic perfusion CT: Explanations by two-compartment model analysis and limited temporal sampling of dynamic CT. J Cardiovasc Comput Tomogr 2016;10(3):207–214.
15. Ichihara T, George RT, Lima JAC, Ikeda Y, Lardo AC. Evaluation of equivalence of upslope method-derived myocardial perfusion index and transfer constant based on two-compartment tracer kinetic model. IEEE Nuclear Science Symposium & Medical Imaging Conference, 2010; 2330–2333.
16. Germino M, Ropchan J, Mulnix T, et al. Quantification of myocardial blood flow with (82)Rb: Validation with (15)O-water using time-of-flight and point-spread-function modeling. EJNMMI Res 2016;6(1):68.
17. Ishida M, Ichihara T, Nagata M, et al. Quantification of myocardial blood flow using model based analysis of first-pass perfusion MRI: extraction fraction of Gd-DTPA varies with myocardial blood flow in human myocardium. Magn Reson Med 2011;66(5):1391–1399.
18. Morita K, Tsukamoto T, Naya M, et al. Smoking cessation normalizes coronary endothelial vasomotor response assessed with 15O-water and PET in healthy young smokers. J Nucl Med 2006;47(12):1914–1920.
19. Salcedo J, Kern MJ. Effects of caffeine and theophylline on coronary hyperemia induced by adenosine or dipyridamole. Catheter Cardiovasc Interv 2009;74(4):598–605.
20. Takafuji M, Kitagawa K, Ishida M, et al. Myocardial coverage and radiation dose in dynamic myocardial perfusion imaging using third-generation dual-source CT. Korean J Radiol 2020;21(1):58–67.
21. Takafuji M, Kitagawa K, Nakamura S, et al. Feasibility of extracellular volume fraction calculation using myocardial CT delayed enhancement with low contrast media administration. J Cardiovasc Comput Tomogr 2020;14(6):524–528.
22. Wisenberg G, Schelbert HR, Hoffman EJ, et al. In vivo quantitation of regional myocardial blood flow by positron-emission computed tomography. Circulation 1981;63(6):1248–1258.
23. Henze E, Huang SC, Ratib O, Hoffman E, Phelps ME, Schelbert HR. Measurements of regional tissue and blood-pool radiotracer concentrations from serial tomographic images of the heart. J Nucl Med 1983;24(11):987–996.
24. Bamberg F, Hinkel R, Schwarz F, et al. Accuracy of dynamic computed tomography adenosine stress myocardial perfusion imaging in estimating myocardial blood flow at various degrees of coronary artery stenosis using a porcine animal model. Invest Radiol 2012;47(1):71–77.
25. Schuirmann DJ. A comparison of the two one-sided tests procedure and the power approach for assessing the equivalence of average bioavailability. J Pharmacokinet Biopharm 1987;15(6):657–680.
26. Kaufmann PA, Gnecchi-Ruscone T, Yap JT, Rimoldi O, Camici PG. Assessment of the reproducibility of baseline and hyperemic myocardial blood flow measurements with 15O-labeled water and PET. J Nucl Med 1999;40(11):1848–1856.
27. Wyss CA, Koepfli P, Mikolajczyk K, Burger C, von Schulthess GK, Kaufmann PA. Bicycle exercise stress in PET for assessment of coronary flow reserve: repeatability and comparison with adenosine stress. J Nucl Med 2003;44(2):146–154.

28. Kikuchi Y, Oyama-Manabe N, Naya M, et al. Quantification of myocardial blood flow using dynamic 320-row multi-detector CT as compared with 15O-H2O PET. Eur Radiol 2014;24(7):1547–1556.
29. Tomiyama Y, Manabe O, Oyama-Manabe N, et al. Quantification of myocardial blood flow with dynamic perfusion 3.0 Tesla MRI: Validation with (15) O-water PET. J Magn Reson Imaging 2015;42(3):754–762.
30. Alessio AM, Bindschadler M, Busey JM, Shuman WP, Caldwell JH, Branch KR. Accuracy of myocardial blood flow estimation from dynamic contrast-enhanced cardiac CT compared with PET. Circ Cardiovasc Imaging 2019;12(6):e008323.
31. Michallek F, Dewey M. Fractal analysis of the ischemic transition region in chronic ischemic heart disease using magnetic resonance imaging. Eur Radiol 2017;27(4):1537–1546.
32. Uren NG, Crake T, Lefroy DC, de Silva R, Davies GJ, Maseri A. Reduced coronary vasodilator function in infarcted and normal myocardium after myocardial infarction. N Engl J Med 1994;331(4):222–227.
33. Renkin EM. Transport of potassium-42 from blood to tissue in isolated mammalian skeletal muscles. Am J Physiol 1959;197(6):1205–1210.
34. Crone C. The permeability of capillaries in various organs as determined by use of the 'indicator diffusion' method. Acta Physiol Scand 1963;58(4):292–305.
35. Nesterov SV, Han C, Mäki M, et al. Myocardial perfusion quantitation with 15O-labelled water PET: high reproducibility of the new cardiac analysis software (Carimas). Eur J Nucl Med Mol Imaging 2009;36(10):1594–1602.